

UNCLASSIFIED

AD NUMBER

AD440607

LIMITATION CHANGES

TO:

Approved for public release; distribution is unlimited.

FROM:

Distribution authorized to U.S. Gov't. agencies and their contractors;
Administrative/Operational Use; MAY 1964. Other requests shall be referred to Office of Naval Research, Washington, DC 20360.

AUTHORITY

onr ltr, 4 may 1977

THIS PAGE IS UNCLASSIFIED

THIS REPORT HAS BEEN DELIMITED
AND CLEARED FOR PUBLIC RELEASE
UNDER DOD DIRECTIVE 5200.20 AND
NO RESTRICTIONS ARE IMPOSED UPON
ITS USE AND DISCLOSURE,

DISTRIBUTION STATEMENT A

APPROVED FOR PUBLIC RELEASE;
DISTRIBUTION UNLIMITED,

UNCLASSIFIED

AD 4 4 0 6 0 7

DEFENSE DOCUMENTATION CENTER

FOR

SCIENTIFIC AND TECHNICAL INFORMATION

CAMERON STATION, ALEXANDRIA, VIRGINIA



UNCLASSIFIED

NOTICE: When government or other drawings, specifications or other data are used for any purpose other than in connection with a definitely related government procurement operation, the U. S. Government thereby incurs no responsibility, nor any obligation whatsoever; and the fact that the Government may have formulated, furnished, or in any way supplied the said drawings, specifications, or other data is not to be regarded by implication or otherwise as in any manner licensing the holder or any other person or corporation, or conveying any rights or permission to manufacture, use or sell any patented invention that may in any way be related thereto.

**Measurement of Fluid Properties for
Magnetoplasmadynamic Power Generators
Fourth Quarterly Technical Summary Report
(1 February — 30 April 1964)**

Contract No. Nonr-4104(00)

Order No.: ARPA 420

Project Code No. 3980

Engineering Department Report No. 3861



**Allison Division
General Motors Corporation
Indianapolis, Indiana**

440607

440607

**Measurement of Fluid Properties for
Magnetoplasmadynamic Power Generators
Fourth Quarterly Technical Summary Report
(1 February — 30 April 1964)**

Contract No. Nonr-4104(00)

Order No.: ARPA 420

Project Code No. 3980

Engineering Department Report No. 3861

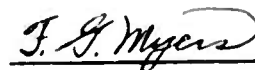
19 May 1964

Written By:



R. T. Schneider,
Program Manager

Approved:



F. G. Myers
Research Director

FOREWORD

This technical summary report was prepared by the Research Department of the Allison Division of General Motors Corporation. The work reported was accomplished under Contract Nonr-4104(00).

The program was sponsored by the Advanced Research and Project Agency through the Power Branch of the Office of Naval Research under the direction of Dr. J. Huth of ARPA and Mr. J. A. Satkowski of ONR.

Allison personnel who contributed material for this report are:

- H. E. Wilhelm
- R. O. Whitaker
- W. Woerner
- R. L. Koch

TABLE OF CONTENTS

<u>Section</u>	<u>Title</u>	<u>Page</u>
I	Introduction	1
II	Resume of Progress	3
III	Test Results	5
	MPD Simulation	5
	Cesium Runs	12
	Runs with Variable Magnetic Fields	15
	Runs with Variable Load Resistor	15
IV	Theoretical Investigations	23
	Ionization in Nonisothermal Plasma	23
	Buildup of Nonequilibrium in a Reacting Plasma Flow with	
	Transverse Magnetic Field	27
	Reactive Relaxation	27
	Transverse Electron Drift	30
	Intercomponent Thermal Nonequilibrium	32
	Application	36
V	Summary for the First Year	39
	Material Problems	39
	Nonequilibrium Ionization	39
	Auxiliary Ionization	39
VI	References	41

LIST OF ILLUSTRATIONS

<u>Figure</u>	<u>Title</u>	<u>Page</u>
1	MPD power simulation setup	5
2	Generated voltage at 1000-ohm load versus velocity	6
3	Generator voltage at 1000-ohm load versus magnetic field	6
4	Typical voltage recording	7
5	Traces of cathode spot on base plate	8
6	Recordings of voltage output with pins heated to 1500°K— 1000-ohm load resistor	9
7	Recordings of voltage output with pins heated to 1620°K— 1000-ohm load resistor	10
8	Recording of voltage output with plate electrodes heated by the gas to 1250°K—5000-ohm load resistor	11
9	Demonstration of the shorting of the intrinsic voltage and the generated voltage by the insulator resistance	13
10	Cesium run with different magnetic fields—100-ohm load resistor	16
11	Voltage output of run shown in Figure 10 versus applied magnetic field	17
12	Cesium run with constant magnetic field and varying load resistors.	17
13	I-V curve of generator for 1400°K gas temperature	18
14	Power output versus load resistance for run in Figure 13	19
15	Directly plotted I-V curves for 1720°K gas temperature	20
16	Directly plotted I-V curves for 1720°K gas temperatures for extreme low and extreme high cesium mass flow. Magnetic field is re- versed between runs I and II	21
17	Electrical conductivity of plasmas—seeding effect	21

1. INTRODUCTION

This fourth Quarterly Technical Summary Report describes the progress made in the period 1 February through 30 April. During this period MPD simulation runs and cesium runs were made.

A considerable amount of data was collected. It was possible to plot a I-V characteristic of the generator directly with an x-y plotter; this is the first direct I-V curve ever taken from a closed loop MPD power generator. Even if we are not sure that we understand all data obtained, we feel that the results are encouraging and a moderate optimism toward the success of closed loop MPD power generation is reasonable.

II. RESUME OF PROGRESS

CONSTRUCTION OF CLOSED LOOP DEVICE

The necessary changes resulting from the experience of the cesium runs previously reported were made during this report period. The cesium injection system was rebuilt so that the cesium flow can be observed and measured through a sight glass.

The cesium-separation system was also improved.

TEST RUNS

A large number of MHD-simulation test runs were made. To do this, the necessary conductivity was created by a high voltage, high frequency discharge with a power input less than one watt. The so-created conductivity was one mho/m, at about 600°K, using helium as working fluid without any seed. Some valuable information was obtained, especially on the influence of external heating of the electrodes on the power output.

Several cesium runs were made at 1400 and at 1700°K. The system operated at these temperatures for several hours without any damage. The data obtained were consistent and reproducible. They are discussed in detail in Section III. Runs at higher temperatures are planned for the near future.

THEORETICAL INVESTIGATIONS

Ionization in Nonisothermal Plasmas

Ionization equations were derived for two-temperature plasmas, when the distribution of the intrinsic atomic states is determined by electron collisions and atomic particle collisions, respectively. The approximations involved in applying the Saha equation to non-equilibrium plasmas are discussed in Section V.

Preliminary investigations have been started toward a theory describing the ionization in plasmas with strong electric fields varying with time.

Allison

Nonequilibrium Processes

A theory describing the establishment of the nonequilibrium in a reacting plasma flow with transverse magnetic field was developed. It is concerned, in particular, with the reactive relaxation, the buildup of the nonequilibrium between the mean mass velocities of the components, and the intercomponent thermal nonequilibrium. The importance relative to the present MPD converter experiment is discussed in Section IV.

III. TEST RESULTS

MPD SIMULATION

The investigations reported in this section were originally initiated to get preliminary information on auxiliary ionization. Because this kind of ionization turned out to be a very convenient way to simulate the condition of Cs seeded He plasma, the setup was used mainly for this purpose.

It is very difficult to run a cesium-seeded system at high temperatures for extended time periods; therefore, the MPD simulation system was used to check the instrumentation. This simulation system provided a conducting helium gas at moderate temperatures without using cesium seeding.

The electrode setup which was used is shown in Figure 1. One plate electrode and one pin electrode, similar to those shown in Figure 7 of EDR 3743 (Third Quarterly Technical Summary Report) were used. The plate was grounded. A pulsed d-c voltage (22 kv, 18 kc) with a power input less than one watt, was applied to the pins of the first row. This created a visible spark between the first pin and the plate electrode. Also, when the helium gas is

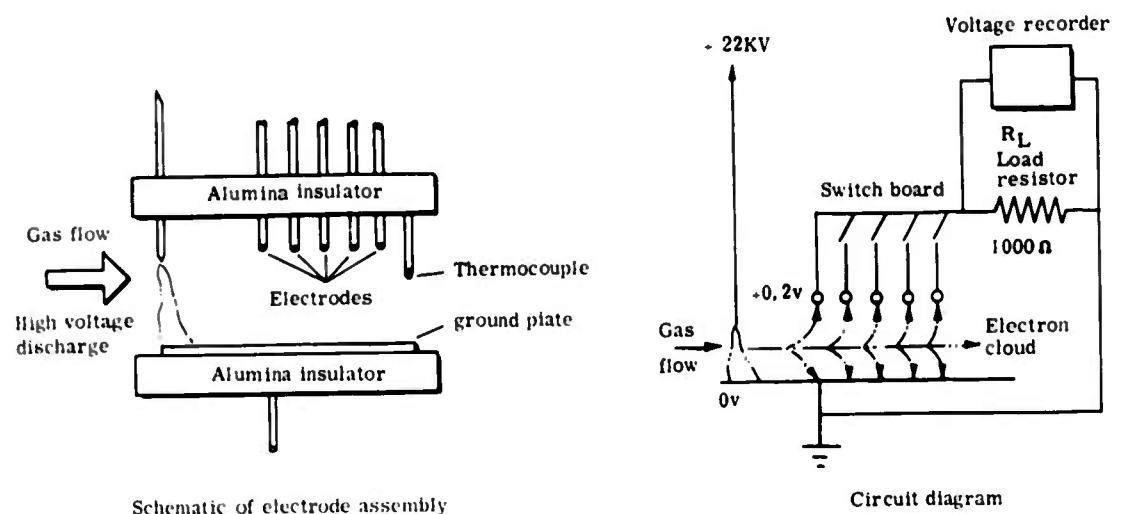


Figure 1. MPD power simulation setup.

flowing, a feeble glow fills the entire interelectrode space. Under these conditions, the conductivity is of the order of one mho/m at 600°K, which is the same order of magnitude as the conductivity which can be expected from thermal ionization at 1800°K when 1% cesium seeding is used.

The MPD-simulation system can be run for days without damaging the electrode or devitrifying the windows, thus allowing complete checkout of all conductivity, spectroscopic, and other instrumentation.

A power output can be drawn from the pins downstream when the magnetic field is applied. Generated voltage at 1000-ohm load is plotted vs velocity in Figure 2. Figure 3 shows the generated voltage measured on one pin, using a 1000-ohm load resistance. The generated voltage seems to be proportional to the magnetic field. The velocity has a greater influence on generated voltage than the first power of velocity as shown in Figure 2.

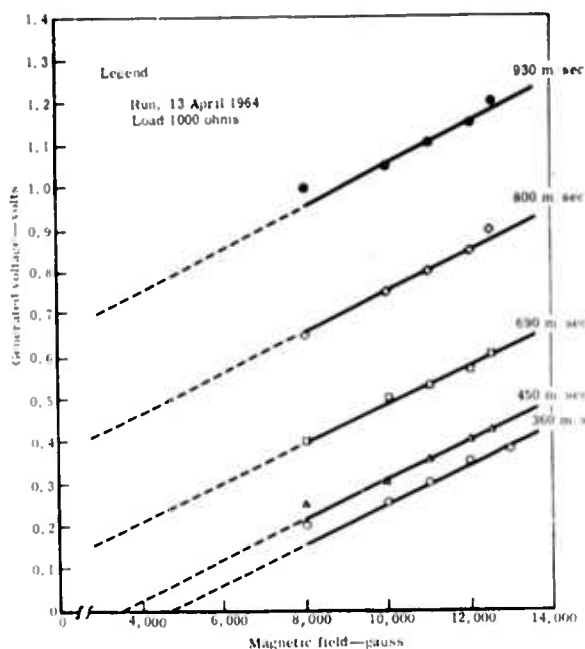


Figure 2. Generated voltage at 1000-ohm load versus velocity.

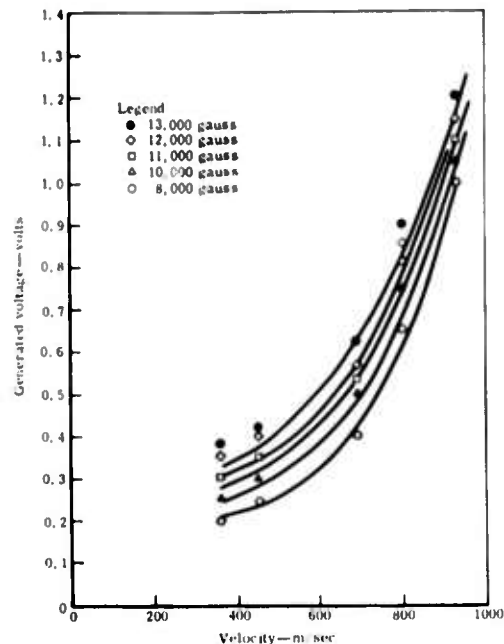


Figure 3. Generator voltage at 1000-ohm load versus magnetic field.

In addition to its usefulness during instrumentation checkout, the MPD-simulation system also provides information relative to the problems associated with MPD power generation. A typical voltage recording is shown in Figure 4. As soon as the high voltage discharge is established, a small output voltage can be measured. This is called the "intrinsic" output. When applying the magnetic field in the positive direction (to augment the intrinsic output), power outputs, as shown in Figures 2 and 3, are obtained. When the magnetic field is reversed, the best result which can be achieved is the reduction of the intrinsic output voltage to zero. A negative output voltage was not observed in this case.

One possible explanation of the aforementioned behavior is as follows. Referring to Figure 3, the gas flow blows electrons downstream from the spark. By diffusion, some of these electrons arrive at the collection pin; many more arrive at the base plate. The latter flow back to the cathode spot in a short loop. The electrons at the collection pin, once captured by the pin, cannot escape because of the high work function of the pin material. These return to the base plate by flowing through the external circuit. This flow constitutes the "intrinsic" output of the device.

When a magnetic field is applied which urges the electrons flowing with the gas stream to move upward and toward the pins, the output power is augmented. When the field is reversed, the electrons are urged downward and

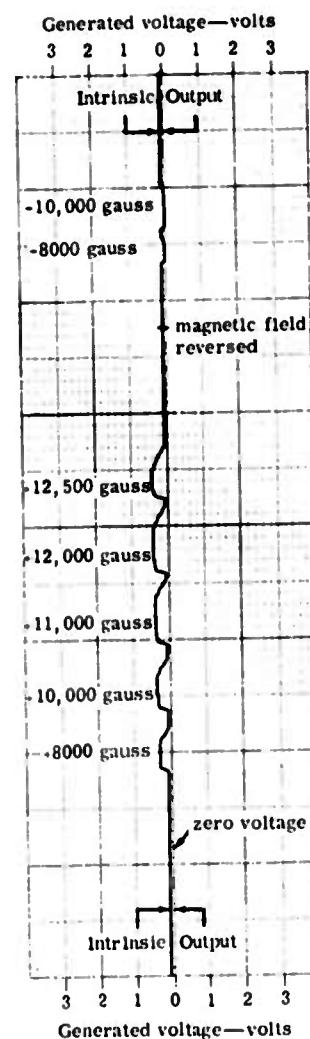


Figure 4. Typical voltage recording.

away from the pins. Thus, the few electrons which would have arrived by diffusion at the collection pin are instead driven away and toward the plate. The output current is reduced to zero because the relatively small induced electric field cannot, of course, cause electrons in the pin to overcome the work function and escape. Consequently, no reverse current develops and the voltage curves of Figures 2 and 3 drop to zero but go no further.

Figure 5 makes it even more clear that electrons are emitted from the plate into the gas stream. Figure 5 shows the traces of the cathode spot of the auxiliary discharge after several hours of running time. The discharge is located on the left side of the picture near the two strong spots. In the time between two pulses the cathode spot is blown downstream, as indicated by the traces.

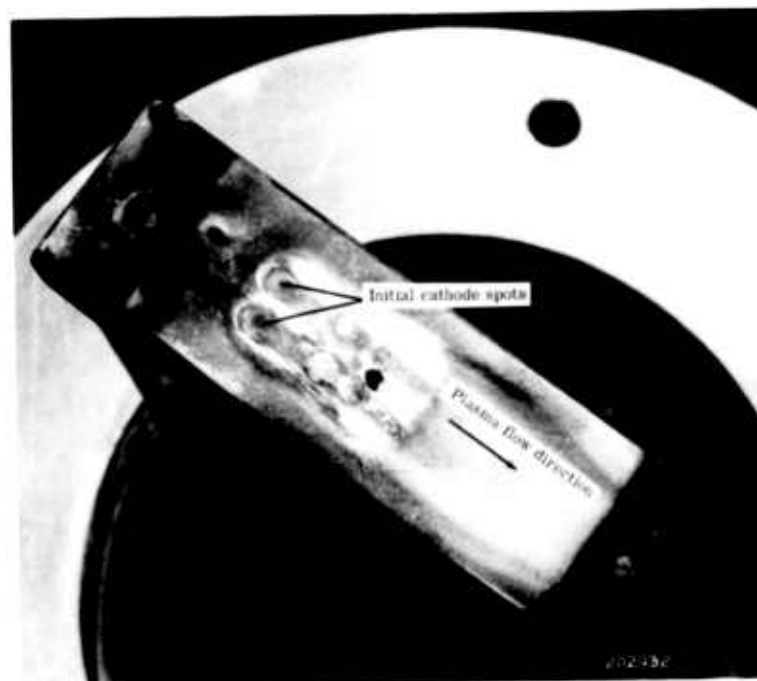


Figure 5. Traces of cathode spot on base plate.

To check the explanation given for the fact that no crossing of the zero line could be observed when reversing the magnetic field, arrangements were made to heat the pins.

When heated to a sufficient high temperature, the pin should be able to emit enough electrons to show a reversed current. Figure 6 shows the result of such a run with the pin heated to 1500°K. The field strength of 13,000 gauss makes the output voltage slightly negative. When heating up to a higher temperature (1620°K) this effect is more pronounced. A typical recording of a run with pins at 1620°K is shown in Figure 7.

The emitting area of a pin is very small (diameter less than one mm). Therefore, it seemed worthwhile to find out how a substantial increase of the emitting area (1:500) would affect the output voltage in the negative direction (output voltage is adverse to intrinsic voltage).

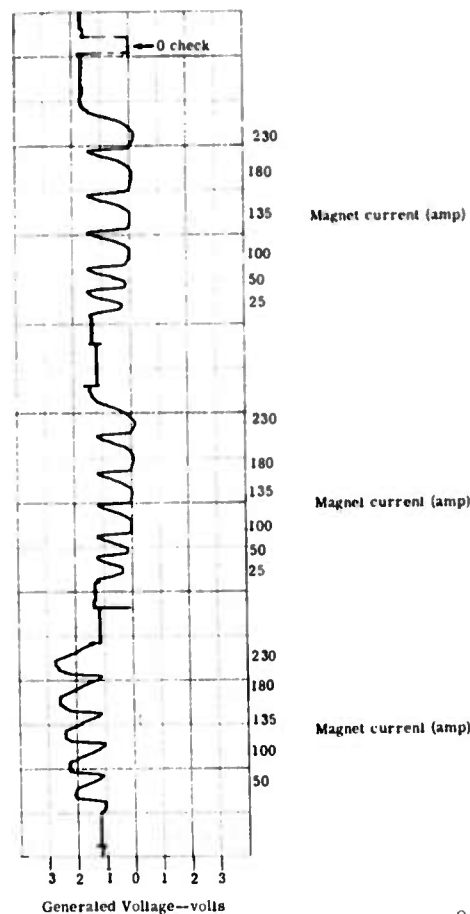
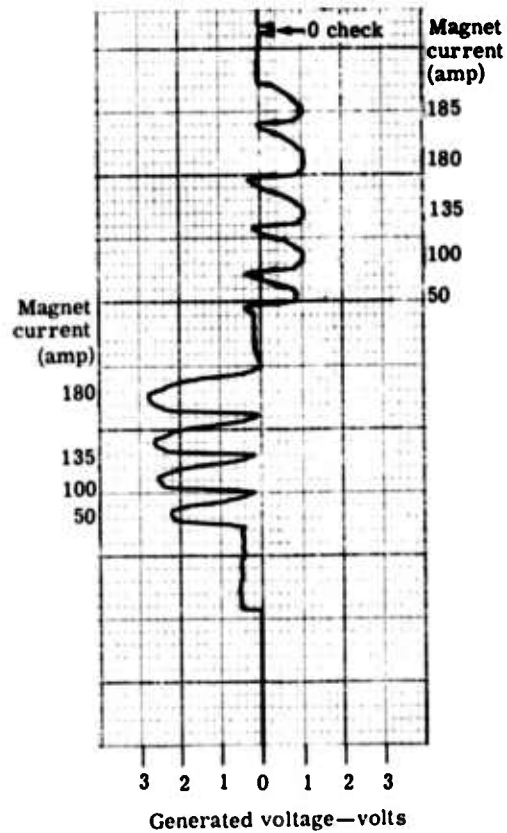


Figure 6. Recordings of voltage output with pins heated to 1500°K—1000-ohm load resistor.

Figure 7. Recordings of voltage output with pins heated to 1620°K—1000-ohm load resistor.



The pins in Figure 1 were replaced by a plate so that two plate electrodes were in the system. In addition to the plate one pin was used which served as anode for the high voltage discharge. This plate was heated by the working fluid up to 1250°K. The results of such a run is shown in Figure 8. The zero line was crossed when the magnetic field was such that output voltage and intrinsic voltage were adverse to each other.

Other valuable information on the behavior of the MPD test section can be derived from recordings of the type shown in Figure 9.

The setup used to obtain data shown in Figure 9 consists of a ground plate and a set of pins as shown in Figure 1. Recordings of the output of one pin are shown for four different gas temperatures (600, 850, 1000, and 1100°K). One fact, derived from Figure 9 is very significant — both output voltage and intrinsic voltage decrease with increasing temperature.

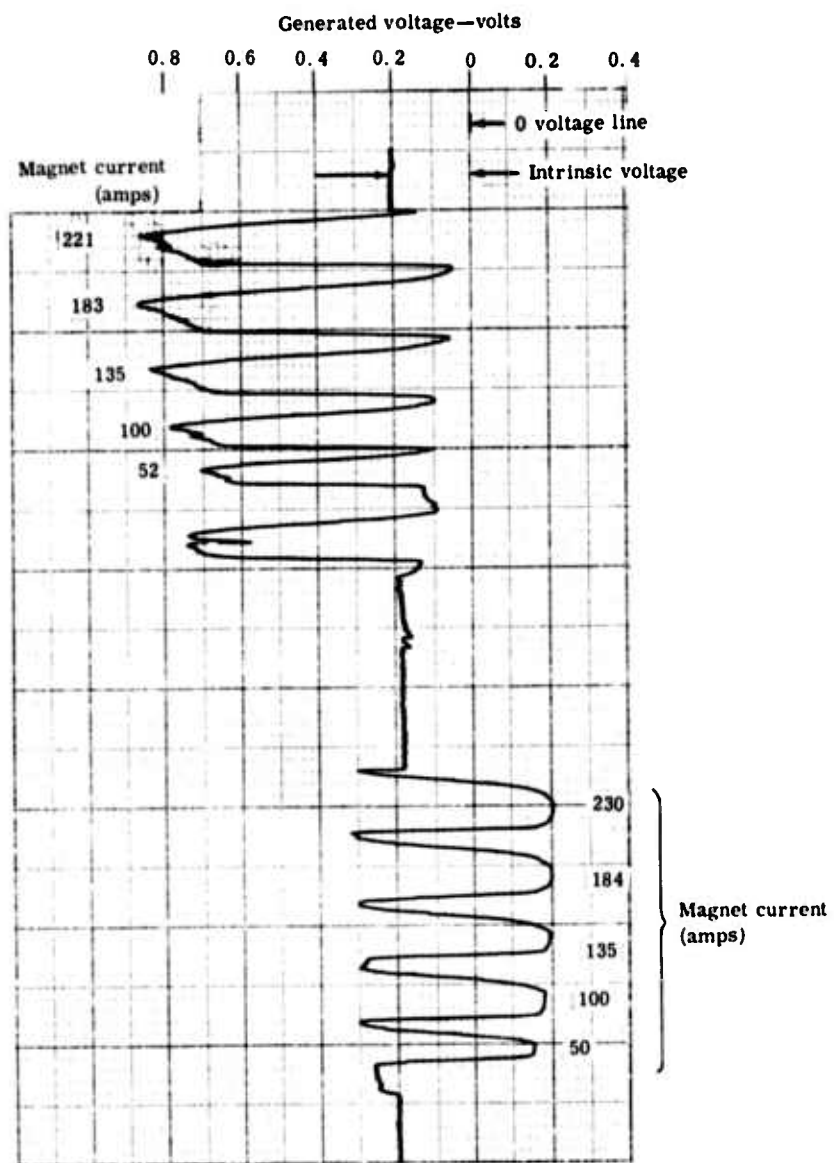


Figure 8. Recording of voltage output with plate electrodes heated by the gas to 1250 K— 5000-ohm load resistor.

The explanation is that the ceramic block which supports the pins becomes a conductor and forms a lead to ground for the output voltage as well as for the intrinsic voltage. For the sake of demonstration, the pin nearest to the metal structure which is connected to ground was chosen. The resistance of the ceramic has to be considered parallel to the external load resistance, which was 1000 ohms. That means the conductivity of the ceramic is quite considerable, and one must be cognizant of this fact when designing a MHD power generator.

In the present setup, only a minor change of design was necessary to account for this conductivity of the ceramic. The ceramic block was mounted differently, so that it is no longer in contact with the gas stream. Pins or plates used as electrodes had to be longer.

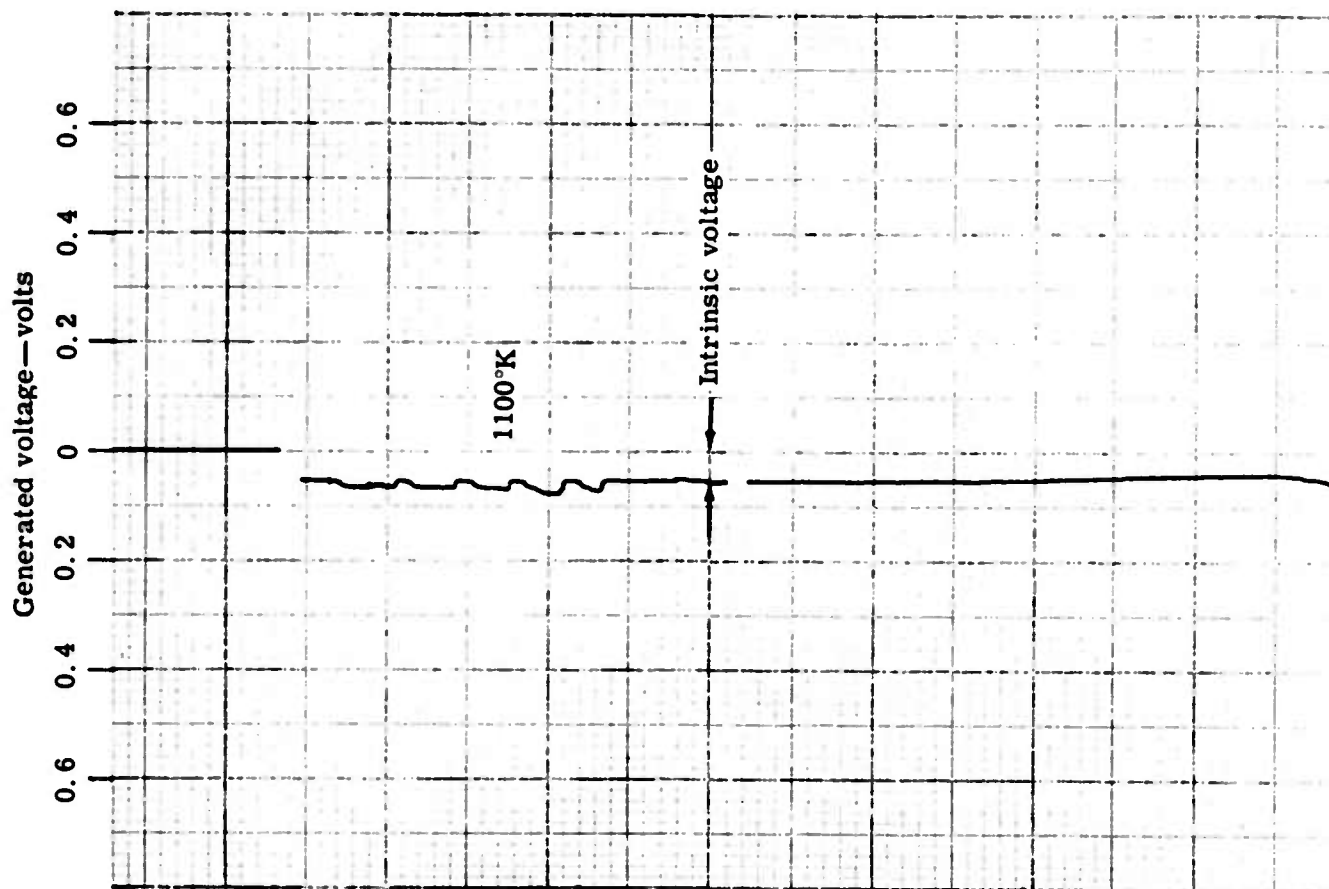
The present load due to conductivity of the ceramic is 20,000 ohms. This is satisfactory for most of the measurements. Still the measurement of the open circuit voltage is not possible.

CESIUM RUNS

Cesium runs were made at two different temperature levels, 1400 and 1720°K. Based on the experience with the MHD-simulation system, three types of electrode configuration were prepared for the runs:

- One pair of plates
- Segmented electrodes with five segments each
- Pin arrangement as described previously

At the present time, the runs with plate electrodes can be regarded as completed for the temperature levels of 1400 and 1720°K. It is anticipated that one more run with plate electrodes at 2000°K will be made at a later time. However, the main interest for closed loop MHD generator is definitely at a temperature level of about 1500°K. Therefore, it is desirable to make more runs first with segmented electrodes and pin electrodes at temperatures between 1400 and 1700°K. At the present time the system is being equipped with segmented electrodes. Minor changes in the support design of the electrode were made to account for the high conductivity of the ceramic material at these temperatures. The runs were made with a static pressure around 1.3 atmosphere in the test section. It is obvious that one could get better conductivities at much lower pressures for this small power output. However, it is believed the information on MHD power generation at



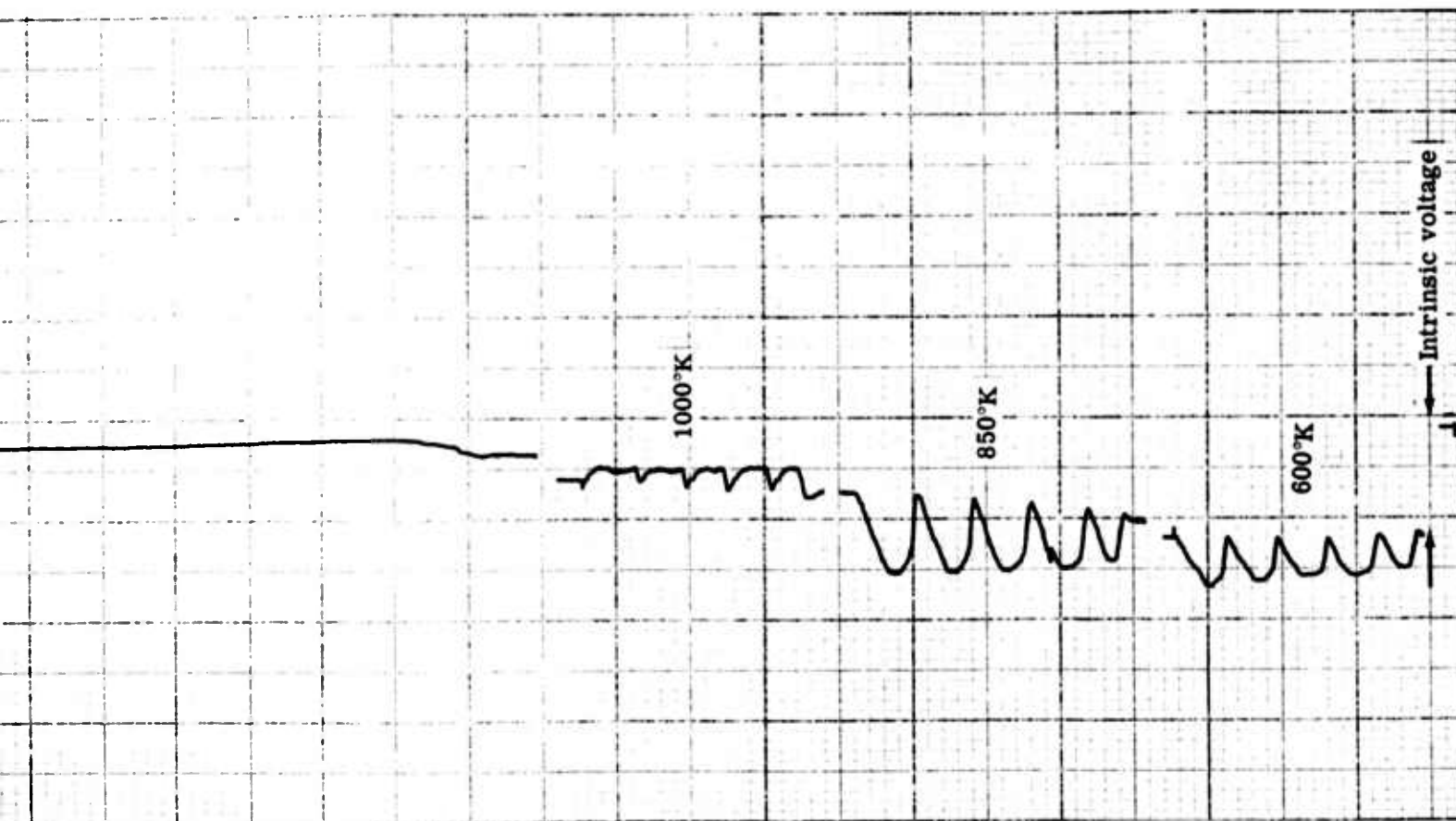


Figure 9. Demonstration of the shorting of the intrinsic voltage and the generated voltage by the insulator resistance.

2

atmospheric pressure and higher is much more valuable from a power density standpoint. Therefore, runs at lower pressure level will be delayed until the present tests are finished.

Typical results from cesium runs with plate electrodes are discussed in the following paragraphs; no attempt has been made to explain these data at this time. An explanation will be presented when more data become available.

RUNS WITH VARIABLE MAGNETIC FIELDS

Figure 10 shows a typical output for a cesium run at 1400°K on a load resistor of 100 ohms using a seeding ratio of 2%. The time scale is 30 sec/in. After establishing the cesium flow, the magnetic field was switched on and current manually increased to the desired level, where it was held for a few seconds and brought back down slowly. Therefore, the shape of the recorded output curve is arbitrary as far as the slope of the curves is concerned. The motor generator for the magnet is wired in such a way that it is possible, when decreasing the magnetic field, to go to slightly negative voltages and thus reverse the field slightly. The effect of this can be seen on the recording, Figure 10, where small peaks in the negative direction appear. The recording also shows an intrinsic voltage of 0.1 volt. There was, of course, no high voltage discharge used for these runs; the intrinsic voltage is, in this case, a pick up from the heater due to the conductivity of the gas. This was observed before and reported in the third quarterly report.

Figure 11 represents a plot of output voltage versus magnetic field for the same run. A proportional increase of the voltage with the magnetic field can only be expected for small load factors; however, the observed saturation should not appear — at least not at such low magnetic fields. As indicated before, no attempt will be made to explain this until additional data has been obtained.

RUNS WITH VARIABLE LOAD RESISTOR

Figure 12 shows a run at 1400°K and 8000 gauss magnetic field where the load resistance was varied. This was one of the first runs and was not a very good one; the results of this run are shown only to indicate the fluctuation in output which were caused by fluctuations in cesium flow. The output follows instantaneously the fluctuations in the cesium flow which should make it feasible to generate a-c current by pulsed injection. More runs are scheduled at a later time to measure the relaxation times for pulsed injection.

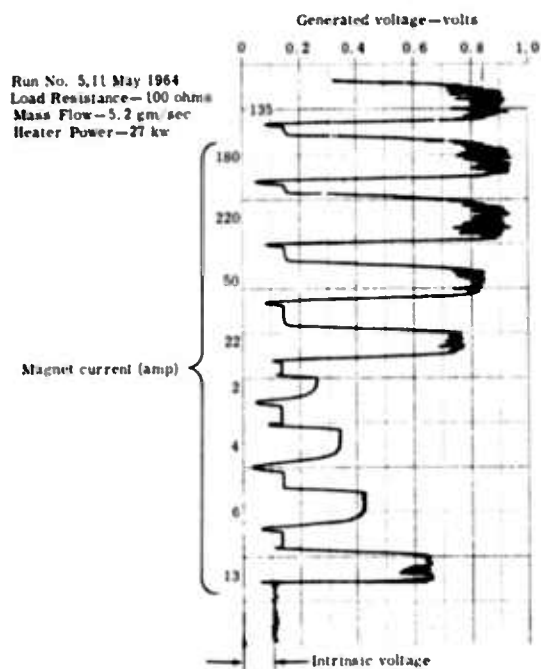


Figure 10. Cesium run with different magnetic fields—100-ohm load resistor.

Figure 13 is an I-V curve derived from data of a run at 1400°K, 10,000 gauss. The numerical values used are listed in Table I. The power output versus load for the same run is shown in Figure 14. After the seeding technique was improved, it became possible to plot I-V curves directly with an x-y plotter when running the experiment.

Table I
Data from a Typical Run (1% Seeding, 10,000-gauss Magnetic Field)

Voltage (volt)	Current (milliamp)	Load Resistor (ohm)	Power ($\times 10^4$ watt)
0.18	3.6	50	6.5
0.24	2.4	100	5.7
0.35	1.75	200	6.1
0.47	0.94	500	4.4
0.54	0.54	1000	2.9
0.64	0.32	2000	2.0
0.68	0.136	5000	0.92

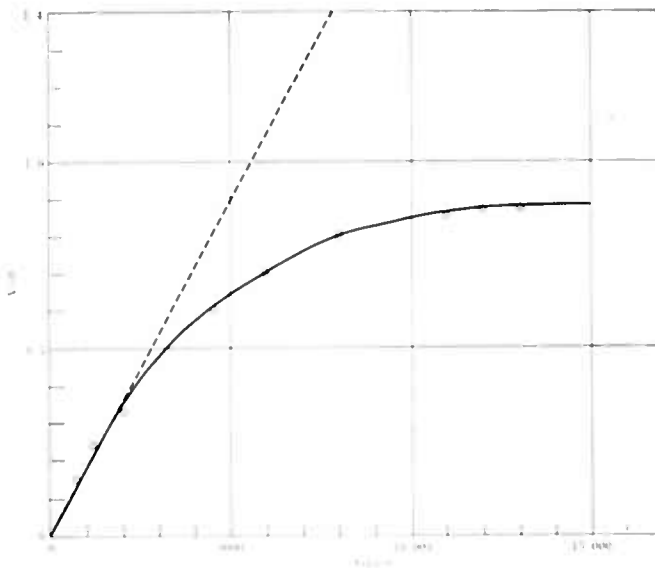


Figure 11. Voltage output of run shown in Figure 10 versus applied magnetic field.

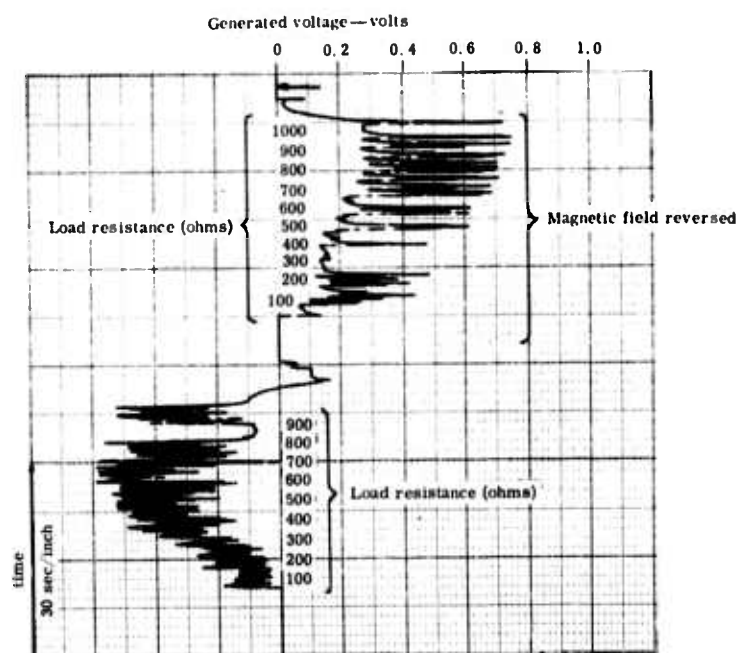


Figure 12. Cesium run with constant magnetic field and varying load resistors.

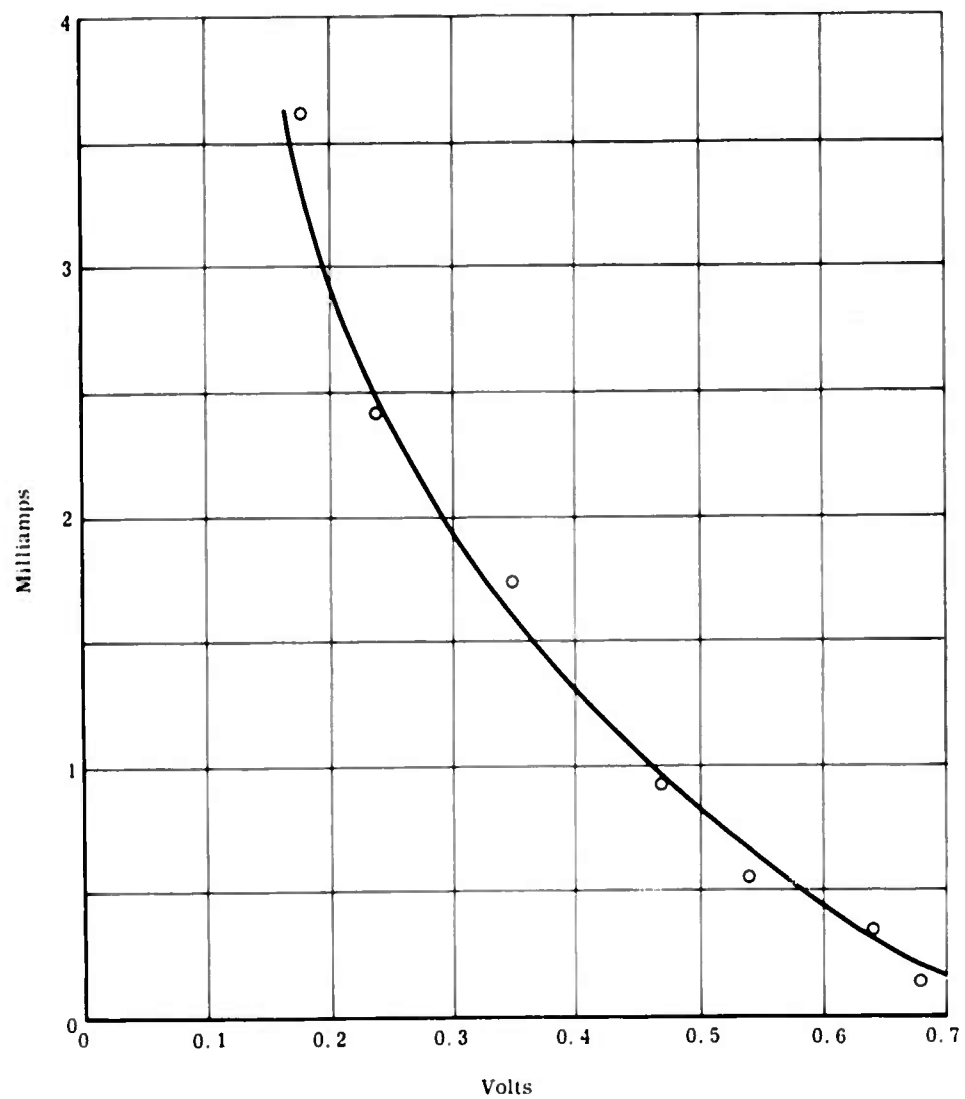


Figure 13. I-V curve of generator for 1400°K gas temperature.

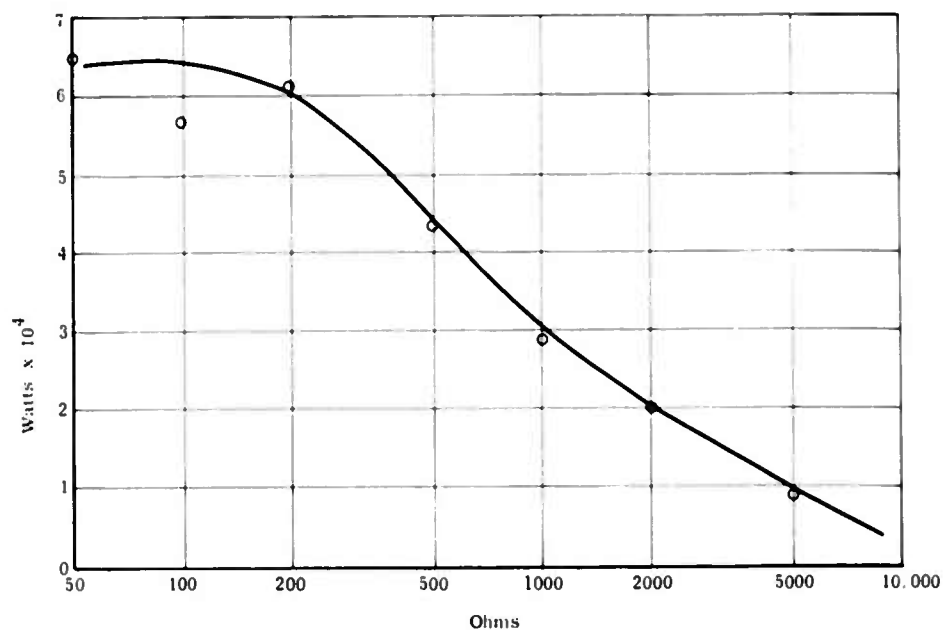


Figure 14. Power output versus load resistance for run in Figure 13.

Two of the I-V curves obtained are shown in Figure 15. All plots were straight lines with superimposed fluctuations. These results seem to be in disagreement with Figure 13 which shows an I-V curve which is not a straight line. The difference between the runs of Figure 13 and Figure 15 is that they are made at different temperatures. The run of Figure 13 was made at 1400°K while the run of Figure 15 was made at 1720°K.

The difference between the two curves in Figure 15 is caused by different cesium mass flows. (1% and 2% seeding ratio).

Another type of information is given in Figure 16. Curve I with the large fluctuation was taken at an extremely low cesium mass flow, while curve II with the small fluctuations was taken with an extremely high cesium mass flow. Curves I and II were taken with the same magnetic field; however, the direction was reversed between curve I and II.

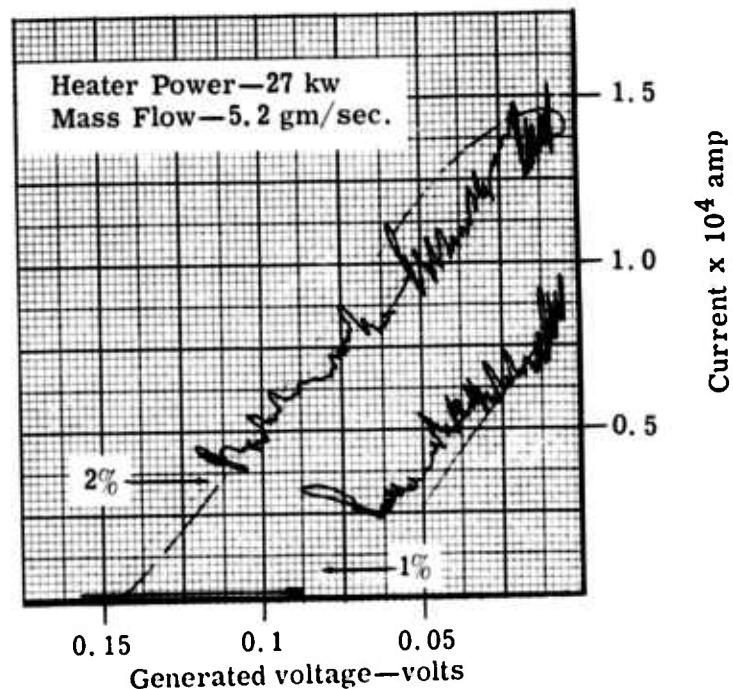


Figure 15. Directly plotted I-V curves for 1720 K gas temperature.

As an aid in understanding this, Figure 17 gives the expected conductivity for different seeding ratios. A small change in the cesium mass flow will cause a large change in power output when the seeding ratio is $< 1\%$ (steep part of the curve in Figure 17) while it will cause only small fluctuation when the seeding ratio is $> 1\%$ (flat part of the curve in Figure 17).

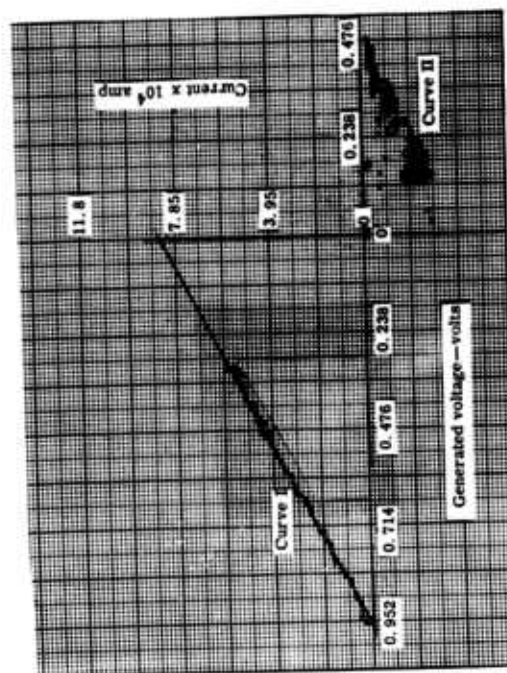


Figure 16. Directly plotted I-V curves for 1720 K gas temperatures for extreme low and extreme high cesium mass flow. Magnetic field is reversed between runs I and II.

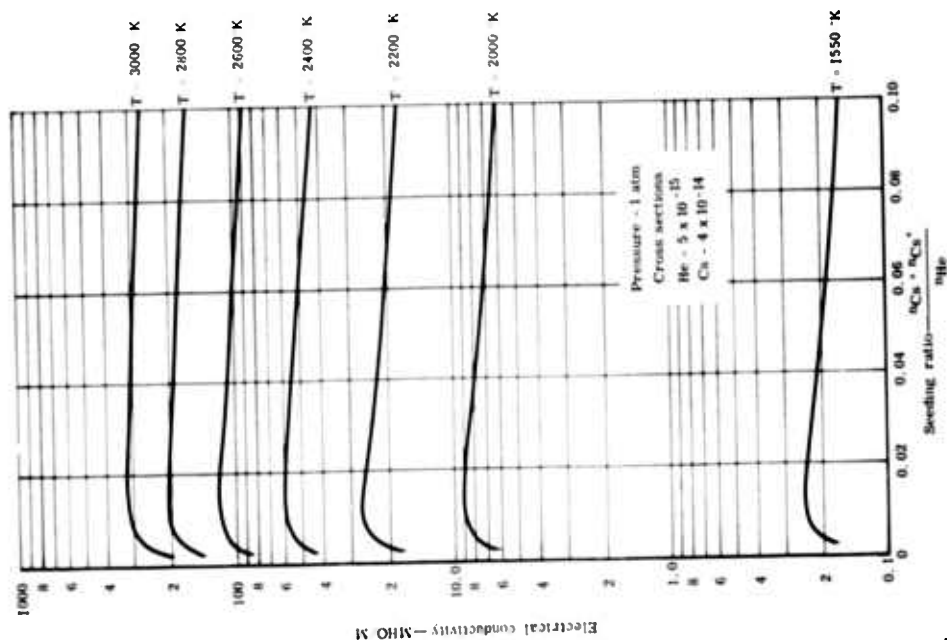


Figure 17. Electrical conductivity of plasmas—seeding effect.

IV. THEORETICAL INVESTIGATIONS

Ionization In Nonisothermal Plasma

In general, it is assumed that an elevated electron temperature considerably increases the degree of ionization in plasma. To investigate the effect of nonisothermic conditions on ionization, assume that approximate local statistical equilibrium is established in the center of mass system of the single plasma components. From the condition of minimum entropy production^{1*}, it results for the stationary ionization state:

$$\sum_s \frac{\mu_s}{T_s} \nu_s = \sum_s \frac{\theta_s}{T_s} \quad (1)$$

The terms on the left side of Equation (1) are associated with the chemical entropy production, the terms on the right side with the thermal entropy production in the plasma. According to the reaction equation,



the stoichiometric coefficients are: $\nu_e = 1$, $\nu_i = 1$, $\nu_a = -1$. For negligible interaction energy compared to the total energy of the particles in the single components, the chemical potentials can be derived in the semiclassical approximation as:

$$\mu_e = -k T_e \left\{ \ln \left[\left(\frac{2 \pi m_e k T_e}{h^2} \right)^{3/2} n_e^{-1} \right] + \ln U_e \right\} \quad (3)$$

$$\mu_i = -k T_0 \left\{ \ln \left[\left(\frac{2 \pi m_i k T_0}{h^2} \right)^{3/2} n_i^{-1} \right] + \ln U_i \right\} \quad \text{and} \quad (4)$$

*Superscripts denote references listed in Section VI

$$\mu_a = -k T_0 \left\{ \ln \left[\left(\frac{2 \pi m_a k T_0}{h^2} \right)^{3/2} n_a^{-1} \right] + \ln U_a \right\}. \quad (5)$$

Note that the individual temperature of the components enters in the translational part of the potentials. The temperatures of the heavy particles, T_i and T_a , have been set equal to a mean gas temperature, T_0 . $U_e = 2$ designates the partition function of the electron spin states. The absolute partition function, U_s , of the atoms and ions, respectively, is related to the excitational partition function, u_s , by ($s = i, a$):

$$U_s = e^{-\epsilon_s/k T} u_s(T), \quad u_s(T) = \sum_{a=0}^{\infty} g_s^a e^{-\epsilon_s^a/k T} \approx g_s^0. \quad (6)$$

where ϵ_s is the energy of the particle in ground state (ϵ_s^a = excitation energy, g_s^a = statistical weight of the a -th state). Obviously, T must be identified with the electron temperature, T_e , or the gas temperature, T_0 , according to the spectrum of the intrinsic states of the atomic particles is determined by electron collisions or atomic particle collisions.

By inserting Equations (3) through (5) into Equation (1), a relation is readily obtained giving the ionizational composition of the plasma. The results are in the cases:

- Distribution of states according to the electron temperature

$$\frac{n_e n_i}{n_a} = 2 \left(\frac{2 \pi m_e k T_e}{h^2} \right)^{3/2} \frac{u_i(T_e)}{u_a(T_e)} e^{-(\epsilon_i - \epsilon_a)/k T_e} e^{+\sum_s \theta_s/k T_s} \quad (7)$$

- Distribution of states according to the gas temperature

$$\frac{n_e n_i}{n_a} = 2 \left(\frac{2 \pi m_e k T_0}{h^2} \right)^{3/2} \frac{u_i(T_0)}{u_a(T_0)} e^{-(\epsilon_i - \epsilon_a)/k T_0} e^{+\sum_s \theta_s/k T_s} \quad (8)$$

In thermodynamic equilibrium, $\sum_s \theta_s / kT_s = 0$ and $T_e = T_0$. Equations (7 and 8) become identical with the Eggert-Saha Equation.

It is recognized that the ionizational composition in a nonisothermal plasma deviates considerably from that in an isothermal plasma when the distribution of the absolute intrinsic particle states is determined by the electron temperature, Equation (7). Under conditions of applicability of Equation (8), i.e., at low electron densities, the nonisothermia affects the ionization relatively insignificantly. It is also noticeable that the thermal nonequilibrium processes enter exponentially, indicating clearly that neglecting them is admissible only at slight nonequilibrium.

In this presentation, the thermal nonequilibrium processes are considered only formally via the expression $\sum_s \theta_s / kT_s$. For idealized models of nonequilibrium plasmas, these thermal nonequilibrium effects on the ionization have been calculated explicitly and will be published soon.

Build-up Of Nonequilibrium
In A
Reacting Plasma Flow With Transverse Magnetic Field

The expansion of a plasma into a region with exterior forcefields is accompanied by both microscopic and macroscopic nonequilibrium processes. These concern the transformation and redistribution of the velocity distributions in the components and the establishment of intercomponent nonequilibrium, respectively. The latter is the subject of the present investigation. The selected theoretical model assumes a slightly ionized plasma flowing into a channel with a transverse magnetic force field and segmented electrodes connected by a Faraday load. The plasma consists of the products of a reacting seeding gas—later referred to by the indices (a) for neutrals, (i) for ions, and (e) for electrons—and a non-reacting driving gas (o). In particular, attention is given to the buildup of the intercomponent thermal nonequilibrium. The investigations are based on the multicomponent field equations of reacting plasmas which were derived from the kinetic equations in the Third Quarterly Report.

REACTIVE RELAXATION

Comparison of the various inelastic collision processes in seeded plasmas at low temperatures shows that the dominant reaction mechanisms are electron collision ionization and three-body electron-ion-electron recombination. As confined to these types of reactions, the reaction equation is:



With Γ^+ as ionization reaction velocity, and Γ^- as recombination reaction velocity, the reactive mass production in the s-component becomes:

$$\left[\frac{d n_s m_s}{d t} \right]_{\text{reactive}} \equiv m_s \sum_{(r, \rho)} \int \left[\frac{d f_s}{d t} \right]_{\text{reactive}} (r, \rho) \cdot d \vec{v}_s = v_s m_s (\Gamma^+ - \Gamma^-) \quad (10)$$

Allison

For the electron component $s = e$: $(r, \rho) = (a, -)$, (i, e) ; and appropriately for the remaining components. The symbol ν_s ($s = e, i, a, o$) designates the stoichiometric coefficients of the reaction, Equation (9), as follows:

$$\nu_e = +2 - 1 = +1, \nu_i = +1, \nu_a = -1, \nu_o = 0. \quad (11)$$

The total reaction velocity, Γ , is given in terms of the (electron collision) ionization probability coefficient,² S_{ea} , and the (three-body electron-ion-electron) recombination probability coefficient,² R_{eie} , by

$$\Gamma \equiv \Gamma^+ - \Gamma^- = n_e n_a S_{ea} - n_i n_e^2 R_{eie}; \quad S_{ea} = S_{ea}(T_e) \quad R_{eie} = R_{eie}(T_e) \quad (12)$$

Under the assumption that the statistical distribution of the internal atomic and ionic states is determined by the electron temperature, the reaction probability coefficients thus defined are functions of the electron temperature alone.

Equation (10) together with Equations (11-12), describes the reactive relaxation phenomena in the components. The substantial derivative is defined by:

$$\frac{d \vec{s}}{dt} = \frac{\partial}{\partial t} + \vec{v}_s \cdot \nabla, \quad \left(\frac{\partial}{\partial t} \equiv 0 \right) \quad (13)$$

It follows—in orders of magnitude—for the characteristic length, in direction of the channel axis, after which:

- The density of the charged particles is changed by a factor $e^{\pm 1}$ [sign according to the sign of: $\nu_{e,i} (n_a S_{ea} - n_e n_i R_{eie})$].

$$l_s^{\text{reactive}} = \frac{\vec{v}_{\parallel s}}{n_a S_{ea} - n_e n_i R_{eie}}, \quad s=e, i \quad (14)$$

- The atom density is changed by a factor $e^{\pm 1}$ [sign according to the sign of:

$$v_a (n_a S_{ea} - n_e n_i R_{eie})]$$

$$l_a^{\text{reactive}} = \left(\frac{n_a}{n_e} \right) \frac{\bar{v}_{ua}}{(n_a S_{ea} - n_e n_i R_{eie})} \quad (15)$$

In particular, the characteristic lengths for the single processes are:

$$l_s^{\text{ionization}} = \frac{\bar{v}_{us}}{n_a S_{ea}}, \quad s = e, i \quad (16)$$

$$l_s^{\text{recombination}} = \frac{\bar{v}_{us}}{n_e n_i R_{eie}}, \quad s = e, i, \quad (17)$$

$$l_a^{\text{ionization}} = \left(\frac{n_a}{n_e} \right) \frac{\bar{v}_{ua}}{n_a S_{ea}} \quad (18)$$

$$l_a^{\text{recombination}} = \left(\frac{n_a}{n_e} \right) \frac{\bar{v}_{ua}}{n_e n_i R_{eie}} \quad (19)$$

The \bar{v}_{us} designate the mean mass velocity of the components (s) parallel to the channel axis. From Equation (14), it may be seen that in reaction equilibrium, $l_{e,i}^{\text{reactive}} = \infty$. This means that the density of the charged particles changes remarkably within a finite length only in the case of strong reaction nonequilibrium.

TRANSVERSE ELECTRON DRIFT

As an experimental arrangement, consider a plasma flowing into a channel with an active section containing a transverse magnetic field and segmented electrodes. The electrodes are connected by a Faraday load R_{\perp} ; their spacing in the transverse direction is designated by L_{\perp} .

In the magnetoactive section of this channel, an intercomponent velocity nonequilibrium which is primarily determined by the electromagnetic forces and intercomponent friction forces is built up. According to the equations of momentum conservation,² this process between two arbitrary components (s) and (r) is described by

$$\begin{aligned} \vec{v}_s \cdot \nabla \vec{v}_s - \vec{v}_r \cdot \nabla \vec{v}_r = & \\ - \frac{8}{3} \sqrt{\frac{2}{\pi}} \left[\sum_{r \neq s} \frac{n_r Q_{sr}}{m_s} \sqrt{\mu_{sr} k T_{sr}} (\vec{v}_s - \vec{v}_r) - \sum_{s \neq r} \frac{n_s Q_{rs}}{m_r} \sqrt{\mu_{rs} k T_{rs}} (\vec{v}_r - \vec{v}_s) \right] & \\ + \frac{e_s}{m_s} \left(\vec{E} + \vec{v}_s \times \vec{B} - \frac{\nabla p_s}{n_s e_s} \right) - \frac{e_r}{m_r} \left(\vec{E} + \vec{v}_r \times \vec{B} - \frac{\nabla p_r}{n_r e_r} \right). & \end{aligned} \quad (20)$$

According to the applying law of collisional interaction, Q_{sr} designates the Ramsauer or Gvosdover³ cross section. The reduced mass and temperature are defined by

$$\mu_{sr} = \frac{m_s m_r}{m_s + m_r}, \text{ and } T_{sr} = \mu_{sr} \left(\frac{T_s}{m_s} + \frac{T_r}{m_r} \right) \quad (21)$$

In the further analysis, the magnetic field of the plasma currents is considered to be small compared to the exterior transverse magnetic field, $\vec{B}_0 (\vec{B} \approx \vec{B}_0)$, and velocity gradients perpendicular to the channel are neglected.

For the considered arrangement, no net Hall-effect exists in the plasma. At relatively small magnetic fields, $\omega_c \tau_c \times \omega_i \tau_i \ll 1$ ($\omega_s = |e_s| B/m_s$, $\tau_s^{-1} = \sum_r \tau_{sr}^{-1}$),

also, ion slip is negligible. In the direction parallel to the channel axis, accordingly, the electron and ion velocity can be taken as equal to the gas velocity: $\bar{v}_{ne,i} = \bar{v}_{na} = \bar{v}_{no}$ (mean downstream mass velocity).

A velocity nonequilibrium is built up in the transverse direction, where under the given conditions $\bar{v}_{ni} \ll \bar{v}_{ie}$. For the latter reason, only the buildup of the transverse electron drift will be investigated in detail. According to Equation (20), this process is described by (\bar{v}_{ne} is replaced by \bar{v}_{no}):

$$\bar{v}_{no} \frac{\partial \bar{v}_{ie}}{\partial x} \approx - \frac{|e_e|}{m_e} \left(\bar{E}_\perp + \bar{v}_{no} \times \bar{B}_0 + \frac{\nabla p_{ie}}{n_e |e_e|} \right) - \frac{8}{3} \sqrt{\frac{2}{\pi}} \left[\sum_{r=o,a,i} \frac{n_r Q_{er}}{m_e} \sqrt{\mu_{er} k T_{er}} + \frac{n_e Q_{oe}}{m_o} \sqrt{\mu_{oe} k T_{oe}} \right] \bar{v}_{ie}. \quad (22)$$

Neglecting terms relatively small of order $m_e/m_r \neq e$, $\frac{n_e m_e}{n_o m_o}$, and the x-dependence of coefficients varying relatively insignificantly in Equation (22), the solution is in first approximation:

$$(\bar{v}_{ie})_x = (\bar{v}_{ie})_{x=0} e^{-x/l_\perp} - \frac{|e_e|}{m_e} \left(\bar{E}_\perp + \bar{v}_{no} \times \bar{B}_0 + \frac{\nabla p_{ie}}{n_e |e_e|} \right) \frac{l_\perp}{\bar{v}_{no}} \left[1 - e^{-x/l_\perp} \right]. \quad (23)$$

where the reciprocal characteristic relaxation length of the process,

$$l_\perp^{-1} = \frac{8}{3} \sqrt{\frac{2}{\pi}} \frac{k T_e}{m_e} \cdot \sum_{r=o,a,i} n_r Q_{er} \cdot v_{no}^{-1}. \quad (24)$$

The finite nonequilibrium state is obtained as the limit $x \rightarrow \infty$ of Equation (23):

$$(\bar{v}_{ie})_\infty = - \frac{|e_e|}{m_e} \left(\bar{E}_\perp + \bar{v}_{no} \times \bar{B}_0 + \frac{\nabla p_{ie}}{n_e |e_e|} \right) l_\perp v_{no}^{-1}. \quad (25)$$

The electric field, \vec{E}_1 , is impressed by the transverse load R_1 , of voltage drop, U_1 :
 $E_1 = -U_1 / l_1$.

From Equation (23), which describes, in rough approximation, the considered process, the following conclusions are reached:

- An arbitrary initial nonequilibrium, $(\vec{v}_{1e})_{x=0}$, would be removed with a relaxation length, l_1 , by intercomponent friction forces.
- In the magnetoactive section of the channel, a nonequilibrium, $\vec{v}_{1e} \neq 0$, is built up which is proportional to the effective field $\vec{E}_1 + \vec{v}_{u0} \times \vec{B}_0 + \frac{\nabla p_{1e}}{n_e |e|}$ acting on the electron component, and shows the x-dependence of a frictional relaxation process of characteristic length l_1 . Practically, after a few relaxation lengths, l_1 , a finite nonequilibrium state is reached (formally designated by a subscript ∞).

A more sophisticated theory of the build up of the electron drift must be based on a microscopic approach.

INTERCOMPONENT THERMAL NONEQUILIBRIUM

The thermal equilibrium between the electron component and the neutral and ionic components is strongly disturbed, as the energy exchange in elastic collisions between electrons and the heavy atomic particles is small. The energy which the electrons acquire in the effective induced electric field of the plasma is, therefore, primarily distributed among the electrons proper, resulting in an elevated electron temperature (electron heating). In the temperature region, where radiation losses are unimportant, the effect is limited by nonradiative, reactive collisions.

In the considered reaction mechanisms, the ionization energy is taken primarily from the electron component, the recombination energy is fed primarily into the electron component. Furthermore, with every transformed s-particle, the energy $\nu_s \frac{3}{2} k T_s$ is liberated in the mean. Consequently, the reactive variation of energy, ΔE_s , of the s-particles is:

$$\Delta E_e = \nu_e \left[\epsilon_n - \frac{3}{2} k T_e \right], \quad \Delta E_i = -\nu_i \frac{3}{2} k T_i, \quad \Delta E_a = -\nu_a \frac{3}{2} k T_a, \quad \Delta E_o = 0. \quad (26)$$

According to the definition of reaction velocities, it follows for the reactive energy production in the s-component:

$$\left[\frac{d n_s \bar{E}_s}{d t} \right]^{\text{reactive}} = \sum_{(r, \rho)} \int E_s \left[\frac{d f_s}{d t} \right]_{(r, \rho)}^{\text{reactive}} \cdot d \vec{v}_s = - \Delta E_s (\Gamma^+ - \Gamma^-). \quad (27)$$

The equation, which describes the buildup of the thermal nonequilibrium between the components (s) and (r) follows from the energy conservation equations² of these components. Considering the reactive energy production and the power of the intercomponent friction forces as the main energy sources, and the intercomponent convective energy exchange (proportional to the temperature difference between the components) as the main inter-component energy distribution mechanism, the result is (δ_{sr} = Kronecker symbol):

$$\begin{aligned} \frac{3}{2} k \left[\vec{v}_s \cdot \nabla T_s - \vec{v}_r \cdot \nabla T_r \right] \approx - \epsilon_n \left[\nu_s \frac{\delta_{es}}{n_s} - \nu_r \frac{\delta_{er}}{n_r} \right] (\Gamma^+ - \Gamma^-) \\ - 8 \sqrt{\frac{2}{\pi}} \left[\sum_{r \neq s} \frac{n_r Q_{sr}}{m_s + m_r} \sqrt{\mu_{sr} k T_{sr}} k (T_s - T_r) - \sum_{s \neq r} \frac{n_s Q_{rs}}{m_r + m_s} \sqrt{\mu_{rs} k T_{rs}} k (T_r - T_s) \right] \\ + \frac{8}{3} \sqrt{\frac{2}{\pi}} \left[\sum_{r \neq s} \frac{n_r Q_{sr}}{m_s} \frac{\mu_{sr}^{3/2}}{\sqrt{k T_{sr}}} k T_s (\vec{v}_s - \vec{v}_r)^2 - \sum_{s \neq r} \frac{n_s Q_{rs}}{m_r} \frac{\mu_{rs}^{3/2}}{\sqrt{k T_{rs}}} k T_r (\vec{v}_r - \vec{v}_s)^2 \right]. \quad (28) \end{aligned}$$

Compared to the relative thermal nonequilibrium of the electron component, the thermal nonequilibrium between the heavy particles is negligible ($T_a \approx T_o$, $T_i \approx T_a$). By consideration of the relative order of magnitude of the mean mass velocities of the components, Equation (28), for the change of the thermal nonequilibrium between the electron and driving gas component in the axial direction, gives:

$$\begin{aligned} \bar{v}_{\parallel o} \frac{3}{2} k \left(\frac{\partial (T_e - T_o)}{\partial x} \right) \approx - \epsilon_n \left[n_a S_{ea} - n_e n_i R_{eie} \right] \\ - 8 \sqrt{\frac{2}{\pi}} \left[\sum_{r=o, a, i} \frac{n_r Q_{er}}{m_e + m_r} \sqrt{\mu_{er} k T_{er}} + \frac{n_e Q_{oe}}{m_o + m_e} \sqrt{\mu_{oe} k T_{oe}} \right] k (T_e - T_o) \\ + \frac{8}{3} \sqrt{\frac{2}{\pi}} \left[\sum_{r=o, a, i} \frac{n_r Q_{er}}{m_e} \frac{\mu_{er}^{3/2}}{\sqrt{k T_{er}}} k T_e - \frac{n_e Q_{oe}}{m_o} \frac{\mu_{oe}^{3/2}}{\sqrt{k T_{oe}}} k T_o \right] \frac{\bar{v}_{\perp e}^2}{2} \quad (29) \end{aligned}$$

As will be verified by the result, the thermal nonequilibrium builds up with a relaxation length l_T which is large compared to the relaxation length l_\perp . Equation (24), of the buildup of the electron drift velocity. In the region above the current buildup, $x \gtrsim 2 \cdot l_\perp$, therefore, the frictional heat source can be regarded as varying relatively insignificantly. Under consideration of these circumstances, Equation (29) can be integrated to give in first approximation:

$$\begin{aligned} \frac{3}{2} k (T_e - T_o)_x &= \frac{3}{2} k (T_e - T_o)_{x=0} e^{-x/l_T} \\ &+ \left[\frac{8}{3} \sqrt{\frac{2 k T_e}{\pi m_e}} \sum_{r=o, a, i} n_r Q_{er} \cdot m_e \bar{v}_{\perp e}^2 - (n_a S_{ea} - n_e n_i R_{eie}) \cdot e_n \right] \frac{l_T}{\bar{v}_{uo}} \left[1 - e^{-x/l_T} \right], \end{aligned} \quad (30)$$

where the reciprocal characteristic relaxation length of the process,

$$l_T^{-1} = \frac{16}{3} \sqrt{\frac{2 k T_e}{\pi m_e}} \cdot \sum_{r=o, a, i} \frac{m_e}{m_r} n_r Q_{er} \cdot \bar{v}_{uo}^{-1} \quad (31)$$

Terms, relatively small of order $m_e/m_{r \neq e}$ and $\frac{n_e m_o T_o}{n_o m_o T_e}$ have been neglected. The finite nonequilibrium state follows as the limit $x \rightarrow \infty$ of Equation (30):

$$\frac{3}{2} k (T_e - T_o)_\infty = \left[\frac{8}{3} \sqrt{\frac{2 k T_e}{\pi m_e}} \cdot \sum_{r=o, a, i} n_r Q_{er} \cdot m_e \bar{v}_{\perp e}^2 - (n_a S_{ea} - n_e n_i R_{eie}) e_n \right] \frac{l_T}{\bar{v}_{uo}}. \quad (32)$$

When the reactive terms are omitted, Equation (32) becomes, in principle, identical with the relation given by Finkelnburg.

Equations (30 through 32) lead to the following conclusions:

An arbitrary initial temperature nonequilibrium, $(T_e - T_o)_{x=0} / 0$ would be removed due to thermal energy transfer between the components according to a relaxation process of characteristic length l_T . This thermal relaxation length, l_T , is of the order $\sum_{r/e} \frac{n_r}{m_e} Q_{er} / \sum_{r/e} n_r Q_{er} \approx \frac{m_o}{m_e}$ larger than the relaxation length, l_\perp , of the velocity nonequilibrium.

After the buildup of the electron drift velocity, which because of $l_\perp \ll l_T$, has been considered to occur here within a relatively negligible length, a thermal nonequilibrium, $(T_e - T_o) / 0$, is built up due to the power liberated by the intercomponent friction forces and reactions in the electron component $\left(\frac{n_e m_e T_o}{n_o m_o T_e} \ll 1 \right)$. This process shows the x-dependence of a relaxation of characteristic length l_T . The finite nonequilibrium is proportional to the total power liberated in the electron component and the "electron heating length" l_T .

For further discussion, define a reactive relaxation length, l^r , which characterizes the reactive change of the electron density and which is positive or negative depending on whether the ionization reaction velocity is larger or smaller than the recombination reaction velocity, by:

$$l^r = \frac{\bar{v}_{io}}{n_a S_{ea} - n_e n_i R_{ei}} \quad (33)$$

By means of the relaxation lengths l_\perp , l_T , and l^r from Equations (24), (31), and (33), Equation (32) can be rewritten in the form:

$$\frac{3}{2} k (T_e - T_o)_\infty = \frac{1}{2} m_e \bar{v}_\perp^2 \cdot \left[2 - \frac{l_\perp}{l^r} \cdot \frac{n}{\frac{1}{2} m_e \bar{v}_\perp^2} \right] \cdot \frac{l_T}{l_\perp} \quad (34)$$

It is recognized that the reactive energy production in the state of reactive nonequilibrium produces an elevation or depression of the intercomponent thermal nonequilibrium, according to whether the reactive relaxation l^r is negative or positive. It is under the conditions:

$$\frac{l_{\perp}}{l^r} \leq 2 \frac{\frac{1}{2} m_e v_{\perp e}^2}{\epsilon_n} : (T_e - T_0)_{\infty} \geq 0 \quad (35)$$

$$\frac{l_{\perp}}{l^r} \geq 2 \frac{\frac{1}{2} m_e v_{\perp e}^2}{\epsilon_n} : (T_e - T_0)_{\infty} \leq 0 \quad (36)$$

In Equations (35 and 36) consider that, in general, $m_e v_{\perp e}^2 / \epsilon_n \ll 1$. In reaction equilibrium, $l^r = \infty$, of course no reactive influence exists, as in this special case no reactive energy production occurs in the plasma.

APPLICATION

The investigated nonequilibrium processes are to be observed in experiment when the relaxation length (l) of the process is not remarkably larger than the active length of the channel (L) . As an example, consider a helium plasma flow seeded with 1% cesium at a mean gas temperature $T_0 = 2000^\circ\text{K}$ and a mean total pressure $P_0 = 1$ atmosphere. The particle constants in this case are:

$$Q_{e0} = 5 \times 10^{-16} \text{ cm}^2, Q_{ea} = 4 \times 10^{-16} \text{ cm}^2, Q_{ei} = 3 \times 10^{-12} \text{ cm}^2$$

$$m_0 = 6.689 \times 10^{-24} \text{ gr}, m_a = 2.172 \times 10^{-22} \text{ gr} = m_i$$

$$m_e = 9.108 \times 10^{-28} \text{ gr}$$

Based on the equilibrium densities at the channel entrance, $n_0 = 3.6 \times 10^{18} \text{ cm}^{-3}$, $n_e = 3.5 \times 10^{13} \text{ cm}^{-3} = n_i$, $n_a = 3.6 \times 10^{16} \text{ cm}^{-3}$, it follows for the order of magnitude of the relaxation length in Equation (31):

$$l_T \approx 8 \times 10^{-8} \bar{v}_{n0} \sqrt{\frac{T_0}{T_e}} \text{ cm}$$

Consequently, for a mean flow velocity of $\bar{v}_{n0} = 10^5$ cm/sec, the characteristic length for the buildup of the thermal nonequilibrium is of the order $l_T \approx 0.8 \times 10^{-2}$ cm. More accurate values can be obtained if necessary by estimating the electron temperature in accordance with Equation (34).

The relaxation length, l^r , for the reactive change of the electron density is considerably larger than the relaxation length of the thermal nonequilibrium. For a nonequilibrium electron temperature $T_e = 3000^\circ\text{K}$ ($T_0 = 2000^\circ\text{K}$), the results from Equation (33):

$$l^r \approx 10^{-4} \bar{v}_{n0} \text{ cm}$$

when reactive nonequilibrium with predominating ionization is assumed. For $\bar{v}_{n0} = 10^5$ cm/sec a relaxation length $l^r = 10$ cm is obtained. Consequently, a nonequilibrium ionization corresponding to the nonequilibrium electron temperature built up in the channel can be observed only above a length of this order of magnitude.

V. SUMMARY FOR THE FIRST YEAR

During the past year a closed loop MPD device was designed, manufactured, and operated. As preliminary conclusions of this research work the following statements can be made.

MATERIAL PROBLEMS

Materials are available to build a closed loop MPD device using cesium as seed material for long-time operation. This has been shown to be true at least up to 1700°K. Such a generator has to be designed very carefully because of the poor insulation properties of alumina, due to high temperature, or due to deposition of impurities or cesium. However, it has been shown that the utilization of exotic materials can be reduced to a minimum.

NONEQUILIBRIUM IONIZATION

The overall conductivity obtained has been of the same order of magnitude as the plasma conductivity due to thermal ionization (0.25 mho/m for 1400°K and 1 mho/m for 1700°K). Since the overall conductivity includes losses in the boundary layers which might be quite substantial, there is a good possibility that a higher conductivity exists than would be expected due to thermal ionization. However, at the present time no quantitative information is available; this information will be obtained in the near future.

AUXILIARY IONIZATION

Encouraging results were obtained at low temperatures with auxiliary ionization by a corona discharge at atmospheric pressure. The conductivity obtained was one mho/m. A more thorough investigation of this effect is required.

VI. REFERENCES

1. Prigogine, I. . Thermodynamics of Irreversible Processes. New York, Interscience Publishers, Inc., 1961.
2. Wilhelm, H. E. . Theoretical Investigations. Third Quarterly Technical Summary Report. Allison Division, GMC, EDR 3743, 1964.
3. Chapman, S. , and Cowling, T. G. . The Mathematical Theory of Nonuniform Gases. Cambridge, 1956.
4. Cowling, T. G. , Magnetohydrodynamics. New York, Interscience Publishers, Inc. . 1957.
5. Finkelburg, W. , and Maecker, H. , "Electric Arcs and Thermal Plasma." Handbook of Physics, Vol. XXII. Berlin, Springer, 1956.

DISTRIBUTION LIST

	<u>No. copies</u>
Director, Advanced Research Projects Agency The Pentagon Washington, D. C. 20301 Attn: Dr. John Huth	2
Office of Naval Research Power Branch (Code 429) Washington, D. C. 20360 Attn: John A. Satkowski	6
Commanding Officer Office of Naval Research Branch Office Box 39 Navy #100 Fleet Post Office New York, New York	1
Cognizant ONR Area Branch Office	1
U. S. Naval Research Laboratory Washington 25, D. C. Attn: Technical Information Division	6
Wright-Patterson Air Force Base Aeronautical Systems Division Ohio Attn: Don Warnock (ASRMFP-2)	1
Air Force Office of Scientific Research Washington 25, D. C. Attn: Dr. Milton M. Slawsky	1
U. S. Naval Ordnance Test Station Propulsion Applied Research Group China Lake, California Attn: Leroy J. Krzycki (Code 4506)	1
Rome Air Development Center Rome, New York Attn: Mr. Frank J. Mellura	1

	<u>No. copies</u>
U. S. Naval Ordnance Laboratory	
NA Division	
White Oak, Maryland	
Attn: Wallace Knutsen	1
Library	2
Defense Documentation Center	
Cameron Street	
Alexandria, Virginia 22314	20
U. S. Army Research & Development Laboratory	
Fort Belvoir, Virginia	
Attn: Frank Shields (ERD-EP)	1
NASA, Lewis Research Center	
21, 000 Brookpark Road	
Cleveland 35, Ohio	
Attn: Wolfgang Moeckel	1
Dr. B. Lubarsky	1
U. S. Atomic Energy Commission	
Division of Reactor Development	
Direct Energy Conversion Section, RD; AED	
Germantown, Maryland	1
Dr. T. Brogan	
AVCO - Everett Research Laboratory	
2385 Revere Beach Parkway	
Everett, Massachusetts	1
Dr. J. Cole	
Department of Aeronautics	
California Institute of Technology	
Pasadena, California	1
Mr. Arthur Sherman	
General Electric - Valley Forge	
Valley Forge Space Technical Center	
Philadelphia 1, Pennsylvania	1

	<u>No. copies</u>
Otto M. Friedrich, Jr. Plasma Dynamics Research Laboratory Department of Electrical Engineering University of Texas, Austin 12, Texas	1
Dr. W. D. Jackson Electrical Engineering Department Massachusetts Institute of Technology Cambridge 39, Massachusetts	1
Dr. Vernon H. Blackman MHD Research Incorporated 1535 Monrovia Street Newport Beach, California	1
Dr. B. C. Lindley Nuclear Research Centre C. A. Parsons & Co., Ltd. Fossway, Newcastle Upon Tyne 6 England	1
Dr. Robert Eustis Thermosciences Division Stanford University Standford, California	1
Mr. John Wright Central Electricity Research Laboratories Cleeve Road, Leatherhead, Surrey England	1
Dr. Richard Schamberg Rand Corporation 1700 S. Main Street Santa Monica, California	1
Dr. Sam Naiditch Unified Science Associates 826 Arroyo Parkway Pasadena, California	1

	<u>No. copies</u>
Dr. W. S. Emmerich Westinghouse Research Laboratories Beulah Road, Churchill Borough Pittsburgh 35, Pennsylvania	1
Dr. R. T. Schneider Allison Division General Motors Corporation Indianapolis, Indiana	1
Dr. D. G. Elliott Jet Propulsion Laboratory Pasadena, California	1
R. J. Donahue Research Laboratories General Motors Corporation 12 Mile and Mound Roads Warren, Michigan	1
Frank Jamesison Research Laboratories General Motors Corporation 12 Mile and Mound Roads Warren, Michigan	1
N. John Stevens Mail Stop 21-5 Lewis Research Center 21000 Brookpark Road Cleveland, Ohio	1
Irving Granet Republic Aviation Corporation Farmingdale Long Island, New York	1

UNCLASSIFIED

UNCLASSIFIED